ADVANCED MATERIALS
www.advmat.de

AI-Driven Electrolyte Additive Selection to Boost Aqueous Zn-Ion Batteries Stability

*Haobo Li, Junnan Hao, and Shi-Zhang Qiao**

In tackling the stability challenge of aqueous Zn-ion batteries (AZIBs) for large-scale energy storage, the adoption of electrolyte additive emerges as a practical solution. Unlike current trial-and-error methods for selecting electrolyte additives, a data-driven strategy is proposed using theoretically computed surface free energy as a stability descriptor, benchmarked against experimental results. Numerous additives are calculated from existing literature, forming a database for machine learning (ML) training. Importantly, this ML model relies solely on experimental values, effectively addressing the challenge of large solvent molecule models that are difficult to handle with quantum chemistry computation. The interpretable linear regression algorithm identifies the number of heavy atoms in the additive molecule and the liquid surface tension as key factors. Artificial intelligence (AI) clustering categorizes additive molecules, identifying regions with the most significant impact on enhancing battery stability. Experimental verification successfully confirms the exceptional performance of 1,2,3-butanetriol and acetone in the optimal region. This integrated methodology, combining theoretical models, data-driven ML, and experimental validation, provides insights into the rational design of battery electrolyte additives.

1. Introduction

Aqueous Zn-ion batteries (AZIBs) have emerged as promising energy storage devices due to their potential for cost-effective and environmentally friendly large-scale applications.[1] Ensuring stability of Zn electrode is crucial for sustained and reliable performance across numerous charge-discharge cycles.[2] While electrolyte optimization is a key strategy, finding effective additives relies on experimental trial-and-error methods, limiting efficient development. However, the reported additive molecules for AZIBs reveal a diverse array of structures and constituent elements.[3] These encompass groups like alcohols, ethers, acids, amine groups, structures including rings and chains, and elements such as C, H, O, N, P, S, F, etc. The broad diversity presents a substantial challenge in identifying trends and principles, making it difficult to conduct mechanism investigations for the purpose of rational design.

Theoretical computational simulation has been successfully applied to energy material and catalyst design, aiming to achieve rational design by establishing universal descriptors related to electrochemical performance and conducting high-throughput calculations.[4] However, this approach is still rarely used in the design of AZIB electrolytes, primarily due to the scale limitations of computational simulation methods. Specifically, through incorporating additive molecular materials into AZIBs, the additive molecules form a Helmholtz double-layer interface structure on the interface. The stability of this structure plays a crucial role in the performances of AZIBs. The influence of additive molecules on battery stability encompasses three aspects: interactions between additive molecules and the Zn electrode surface, interactions among additive molecules, and interactions between additive molecules and water (**Scheme 1**). Traditional molecular dynamics simulations focus on the latter two interactions,[5] with limited accuracy, while the more precise density functional theory (DFT) calculations of adsorption energy concentrate on interactions between additive molecules and the Zn electrode surface.[6] Incorporating all three factors simultaneously in DFT modelling would result in a substantial computational load. Therefore, theoretical research in this area remains challenging.

The rapid advancement of artificial-intelligence (AI) technology offers promising solutions to this challenge and has been recently applied to design the electrolyte of lithium metal batteries.[7] For problems involving highly complex molecular compositions and structures, machine learning (ML) methods can be employed to predict performance based on physical properties.[8] Additionally, AI clustering[9] can partition extensive theoretical data, helping to identify which experimental data correspond to specific regions, thereby generating domain knowledge and correlating theory with experiment. This approach has been successfully applied to complex issues such as catalytic selectivity.[10] Consequently, we propose a data-driven strategy to select electrolyte additive molecules for AZIBs, offering new insights into electrolyte design methods.

In this work, we first conduct DFT calculations by building an integrated model of full coverage of additive molecules and

H. Li, J. Hao, S.-Z. Qiao
School of Chemical Engineering
The University of Adelaide
Adelaide, SA 5005, Australia
E-mail: s.qiao@adelaide.edu.au

The ORCID identification number(s) for the author(s) of this article can be found under https://doi.org/10.1002/adma.202411991

DOI: 10.1002/adma.202411991

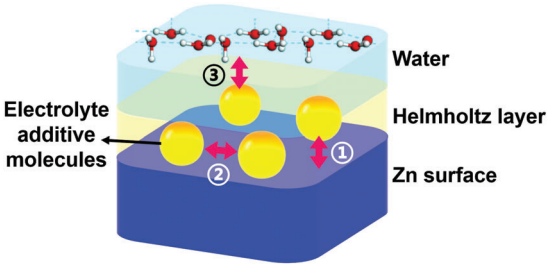

Scheme 1. Interactions for additive molecules in aqueous Zn-ion batteries (AZIBs): ① between additive molecules and the Zn electrode surface; ② among additive molecules; and ③ between additive molecules and water.

water molecules environment on the Zn(002) surface, using fine-tuned accelerated molecular simulations to speed up the process. We find that the surface free energy (γ) of this theoretical model can serve as a descriptor for the experimental reversibility of Zn electrode. We then calculate the γ values for 38 electrolyte additive molecules with different structures and compositions, based on extensive literature reports, and use physically-inspired linear regression ML methods to predict the γ values of 27 additional molecules. AI clustering based on physical features is employed to identify the optimal region for additive molecule selection, combined with γ values. Importantly, we experimentally verify the optimal additive molecules 1,2,3-butanetriol and acetone selected by AI, finding that they significantly improve the stability and electrochemical performance of AZIBs. This methodology combines quantum chemistry simulation, ML prediction, AI screening, and experimental validation, demonstrating its practicality in battery experiments and its potential for wider application in other electrolyte design systems.

2. Results and Discussion

To establish a rational theoretical model, we benchmarked the results of different theoretical models with experimental results reported in the literature.[11] We selected six experimental reports with relatively similar test conditions to ensure that the battery stability test results were comparable (Table S1, Supporting Information). **Figure 1a** summarizes the additive molecules used in these six experiments, encompassing a variety of molecular properties, including size, elemental composition, and functional groups. Identifying general rules from this diverse set is quite challenging.

To comprehensively account for the three interactions outlined in Scheme 1, we constructed the theoretical model shown in Figure 1b. This model uses the most stable Zn(002) surface as the substrate with a larger unit cell size (4 × 4) to accommodate a full layer of additive molecules. The number of additive molecules per unit cell varies based on the size and shape of the molecules to ensure interaction without overcrowding. For example, the smallest methanol has six molecules per unit cell, medium-sized 2-propanol has three, and the larger glucose has one. This setup allows us to consider interactions between additive molecules, between additive molecules and the Zn surface, and between additive molecules and water molecules. A water molecule layer is added above the additive layer to include interactions with H_2O molecules. Due to the large model size, we used the FINETUNA[12] package for fine-tuning accelerated molecular simulations.

The surface free energy (γ) was calculated to present the stability of the surface structure by computing the averaged per unit area, where more negative γ values indicate more stable structures. We observed that γ correlates well with experimental stability results, i.e., Coulombic efficiency of Zn electrode[13] during battery cycling, and fits well with a quadratic polynomial fit. Therefore, γ can be used as a descriptor of battery stability. In contrast, the adsorption energy (E_{ad}) calculated by conventional DFT uses the model shown in Figure 1c. This model does not consider interactions between additive molecules or between additive molecules and H_2O molecules. When considering a wide range of molecular properties, this leads to significant deviations from experimental stability. For instance, E_{ad} of larger molecules like glucose is more negative due to the strong van der Waals forces with the surface, and methanol shows weak bonding to the surface, both obviously inconsistent with experimental results. Based on these findings, we selected the Helmholtz double-layer interface structure formed by additive molecules on the Zn surface, with an explicit aqueous solution layer, as our theoretical model. We then calculated γ of this model as the descriptor of AZIB stability.

Based on the theoretical model described above, we calculated the γ values of 38 additive molecules (**Figure 2d**) reported in the literature,[11,14] to construct a comprehensive database for ML training to predict AZIBs stability. The dataset includes a variety of functional groups, various molecular sizes and shapes, and different elemental compositions. This high diversity allows to reflect the complexity of electrolytes in actual applications, ensuring that the trained ML model can capture a wide range of physicochemical features and predict performance across different types of additive molecules for practical use. All computational models and optimized structures are detailed in Figure S1 (Supporting Information). We selected 17 physical quantities that affect the molecular properties as primary features for ML prediction (**Table 1**). These include molecular properties such as molecular weight, polarizability, the number of atoms of different elements, the number of valence electrons, and the number of H-bond donors and acceptors. Additionally, we considered the average values of atomic properties within the molecules, such as average Pauling electronegativity, average ionic potential, and average electron affinity. We also identified 27 additional molecules (Table S2, Supporting Information) as the prediction set. For detailed database, please refer to Table S3 (Supporting Information) in the Supporting Information.

Figure 2a shows the correlation between each pair of primary features. In most cases, the correlation between these features is low, making them suitable for ML training. Notably, all features selected in this work are easily obtainable through experiments without requiring further DFT calculations. This approach not only facilitates generalization to a broader range of applications but also addresses the challenge of accurately calculating properties for some molecules, such as those with large size. For example, molecule No. 46 in Table S2 (Supporting Information), $C_{36}H_{60}O_{30}$, cannot be simulated by the computational model used in this work due to its large size but can be predicted by this ML method.

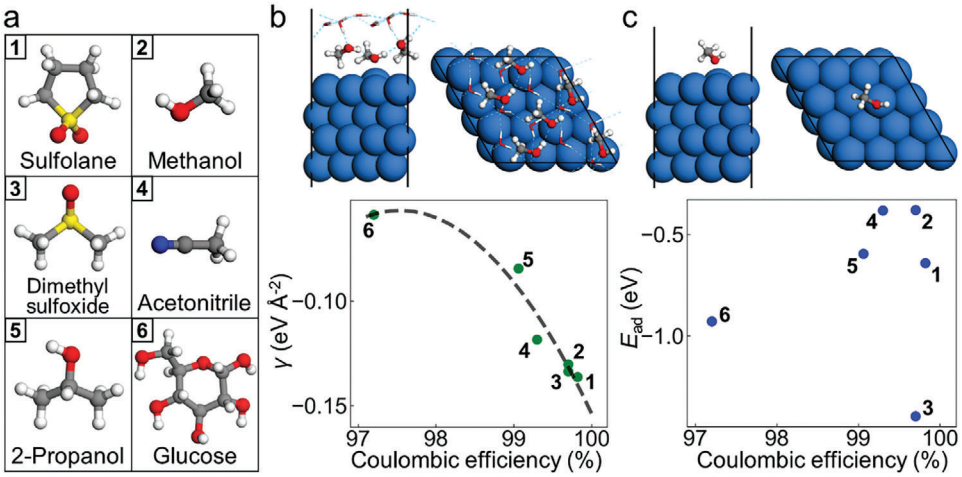

Figure 1. Benchmarking the theoretical descriptor with experimental results. a) Additive molecules reported in the literature.[11] b) Theoretical calculated surface free energy (γ) of the Zn(002) surface with electrolyte used as descriptor for AZIB experimental stability, compared to c) calculated adsorption energy (E_{ad}) of the additive molecule on the Zn(002) surfaces used in traditional methods. The stability is represented in terms of Coulombic efficiency, with the quadratic polynomial fit between γ and Coulombic efficiency shown as the dashed line. Different computational models (side and top views) are illustrated for each method, using ethanol additive as an example. Zn, blue large spheres; C, grey small spheres; O, red small spheres; N, blue small spheres; S, yellow small spheres; H, white small spheres.

We used the SISSO[15] method based on linear regression to predict the γ value. This method identifies the best features and predicts the target quantity, i.e., the γ value, through a formula involving mutual operation between features. Figure 2b shows the order of the influence of different features on γ. The most influential feature is the number of heavy atoms (#HA), followed by surface tension (σ), average ionic potential (AVE_IP), the number of hydrogen bond acceptors (HBA), the number of hydrogen bond donors (HBD), and the ratio of the number of heavy atoms to the number of hydrogen atoms (#HA/#H). These insights provide valuable ideas for designing additive molecules. Interestingly, the 6 most relevant features encompass microscopic molecular properties (#HA, HBA, HBD), atomic properties (AVE_IP), and macroscopic liquid properties (σ). This highlights the complexity of factors influencing the selection of electrolyte additive molecules.

To further explore the relationship between γ and the two primary features, #HA and σ, γ against these variables was plotted in Figure S3 (Supporting Information). The gradual variation of γ with both #HA and σ indicates that electrolyte stability is influenced by both chemical structure (#HA) and physical interactions (σ). Specifically, a lower #HA and higher σ correspond to a lower γ, i.e., a more stable electrolyte. Fewer heavy atoms result in a denser molecular arrangement, while higher surface tension strengthens molecular interactions. These factors together promote the formation of a stable Helmholtz layer on the electrode surface, enhancing the stability of AZIBs.

Figure 2c shows the comparison between the γ values predicted by SISSO and the DFT-calculated values. The dots align closely with the perfect correlation line, with a low root mean square error (RMSE) of 0.045 eV Å^{-2}, demonstrating that the ML method has a certain accuracy and its predicted γ values are reliable for practical application.

Given that molecular properties span multiple aspects, all of which can have complex effects on the performance of AZIBs, we employ an AI-assisted strategy to screen and design additive molecules. First, we reduce the dimensionality of 17 physical quantity features. The random trees embedding (RTE)[16] algorithm reduces these 17 dimensions to two-dimensional mapping, allowing the distribution of additive molecules to be visualized. We use color to represent the descriptor of AZIB stability, γ, where colors towards blue direction indicate greater stability. Then, the K-Means[17] clustering method is applied to perform Voronoi partitioning based on the data point positions. Our basic assumption is that data points within the same zone, having similar positions, are considered to have similar comprehensive physical properties and thus similar effects on AZIB performance.

The optimal number of K was determined through silhouette analysis[18] for K-Means clustering. Silhouette coefficients for K values ranging from 2 to 15 were calculated, with higher values (closer to 1) indicating better separation between clusters. As shown in Figure S2 (Supporting Information), K = 9 was identified as a local maximum, significantly above the average, and was thus selected for **Figure 3**. This choice was further validated by domain knowledge, where K = 9 resulted in well-clustered data points with similar AZIB stability descriptors (γ values), providing meaningful physical interpretations of the additive molecules. For the 38 additives in the ML training set, the DFT-calculated γ values show a correlation with their partition positions. As shown in Figure 3a, γ values in the upper region of the map are usually higher, indicating poor AZIB stability, while the γ values in the three regions in the lower right corner (marked in pink) are lower, indicating good AZIB stability. Therefore, the principle of designing additives is to select molecules from the three AI-selected regions in the lower right corner.

Next, we added the 27 ML-predicted molecules (Figure 3d) to the RTE mapping and AI clustering. As shown in Figure 3b, the predicted γ values (indicated by the color of data points within black circles) also strongly correlate with their respective

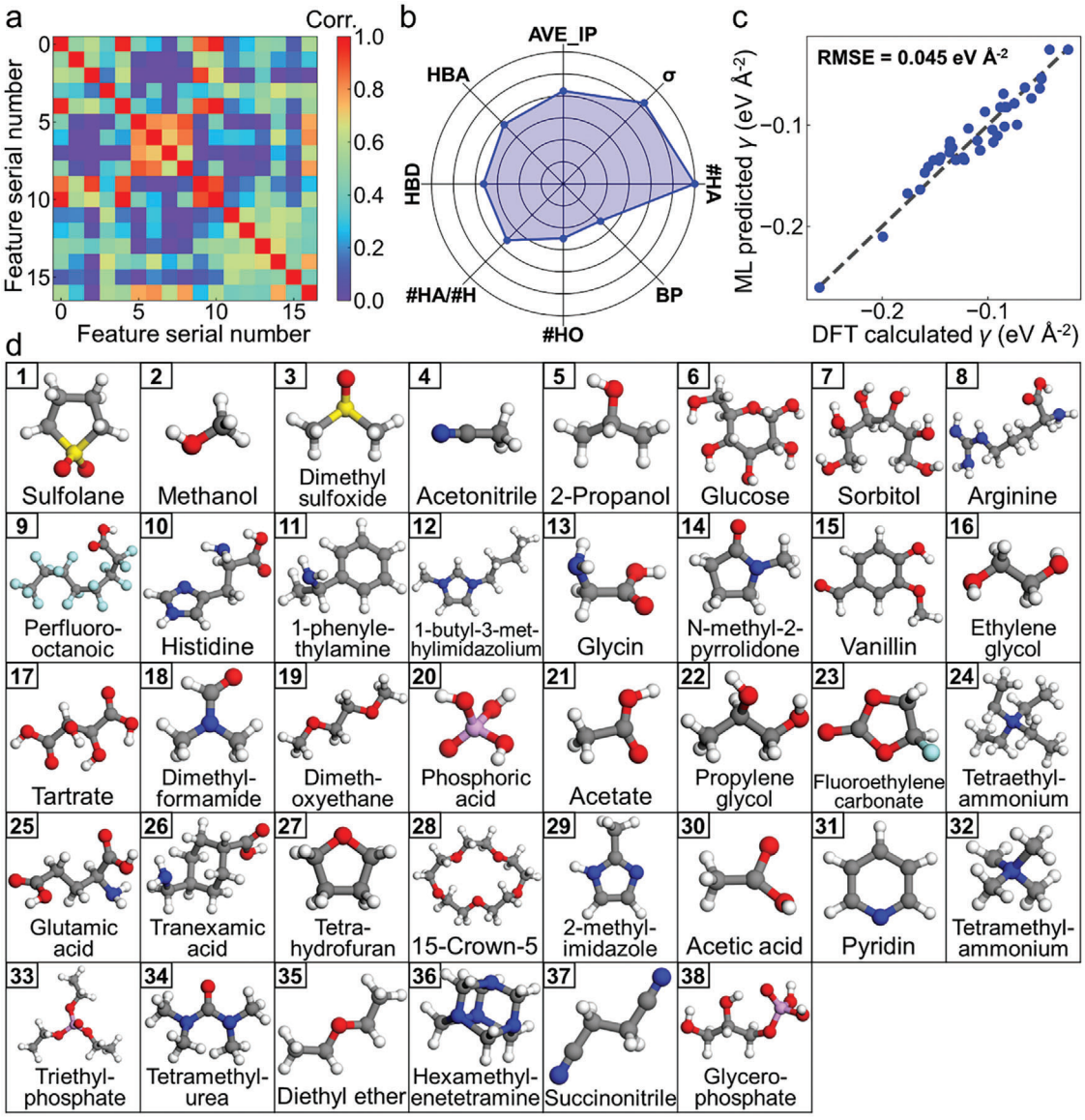

Figure 2. ML prediction for surface free energies (γ) of electrolyte additives. a) Pearson correlation analysis heat map of the 17 molecular features used in this work. b) Top 10 most-correlated features. The distance of each dot from the center is proportional to its correlation coefficient. c) SISSO predicted γ versus DFT calculations of the 38 additive molecules in the database. The root mean square error (RMSE) is calculated as a 5-fold cross-validation prediction error. d) 38 additive molecules computed as the database for ML training. C, grey small spheres; O, red small spheres; N, blue small spheres; P, pink small spheres; S, yellow small spheres; F, cyan small spheres; H, white small spheres.

partitions. The pink regions, indicating good AZIB stability, generally have lower γ values, whereas regions indicating poor stability have higher γ values.

Regarding the AI algorithms, based on the research goals and the nature of the problem, a combination of supervised (SISSO) and unsupervised (RTE and K-Means) methods are chosen. SISSO predicts γ values using known molecular properties in order to develop a predictive model grounded in experimental data and physical-meaningful features, facilitating direct correlation with the target property γ. RTE and K-Means clustering explore the underlying structure of the dataset without predefined labels. This allows the grouping of additive molecules based on their physical properties, revealing clusters that exhibit similar behavior in stabilizing Zn-ion batteries. By visualizing the partitioning of additives, the specific regions are identified more likely to enhance stability, providing additional insights beyond the individual predictions from the supervised model.

The combination of bothapproaches is beneficial for generating a comprehensive view of the system. Supervised learning provides accurate predictions of individual additive performance, while unsupervised learning reveals broader trends and patterns in the dataset, guiding the rational selection of new additives. The consistency between both methods underscores that the simulated performance of AZIBs is driven by the inherent properties of the additives, rather than the AI algorithms, confirming the reliability of the methodology.

Table 1. 17 physical properties as primary features used to describe the electrolyte additive molecules.

Physical property	Classify	Abbreviation	Unit
Molecular weight	Molecular	M	Kg mol^{-1}
Polarizability	Molecular	α	Å^3
Number of H atoms	Molecular	#H	None
Number of O atoms	Molecular	#O	None
Number of heavy atoms	Molecular	#HA	None
Ratio of heavy atoms to hydrogen atoms	Molecular	#HA/#H	None
Number of atoms	Molecular	#A	None
Number of valence electrons	Molecular	n_e	None
H-bond donor	Molecular	HBD	None
H-bond acceptor	Molecular	HBA	None
Average Pauling electronegativity	Atomic	AVE_PE	None
Average ionic potential	Atomic	AVE_IP	eV
Average electronic affinity	Atomic	AVE_EA	eV
Surface tension	Liquid	σ	N m^{-1}
Melting point	Liquid	MP	K
Boiling point	Liquid	BP	K
Density	Liquid	ρ	kg m^{-3}

Finally, we sorted the ML prediction results from the pink area, indicating good AZIB stability, and identified the top 7 molecules with the lowest γ values as the good AI-selected additive molecules (Figure 3c). The most effective molecules are 1,2,3-butanetriol and acetone, which not only fall within the best partition but also have predicted γ values as low as −0.17 eV Å^{-2} and −0.14 eV Å^{-2}, respectively.

To verify the AI prediction results, we selected two predicted electrolyte additive molecules from Figure 3 and 1,2,3-butanetriol and acetone, and conducted experimental verification. The Zn/Cu cells with pure 2 M $ZnSO_4$, 2 M $ZnSO_4$ + 10 v/v% acetone and 2 M $ZnSO_4$ + 10 v/v% 1,2,3-butanetriol were assembled. Initial charge-discharge voltage profiles under 0.5 mA cm^{-2} and 0.5 mA h cm^{-2} were compared. As shown in **Figure** 4a–c, a low initial Coulombic efficiency of 71.4% with a high voltage polarization of 272 mV was obtained for the cell with pure $ZnSO_4$ electrolyte, indicating the poor reversibility of Zn anode in such electrolyte due to the corrosion, hydrogen evolution, and dendrite formation. In comparison, within the electrolyte containing acetone additive, a higher initial Coulombic efficiency of 90.1% with lower voltage polarization of 192 mV was obtained. This indicating the Zn reversibility was enhanced by suppressing the side reactions. Importantly, the cell with butanetriol additive showed the similar electrochemical performance, aligning well with our AI prediction results.

Figure 4d exhibited the cycling stability of symmetric cells with different electrolytes under the low current density of 0.5 mA cm^{-1}. The cell with pure $ZnSO_4$ electrolyte showed significant Coulombic efficiency fluctuation after running for 300 cycles with an average of 96.4%, resulting from the short circuit caused by dendrite growth. In contrast, after introducing acetone and 1,2,3-butanetriol additives to the electrolyte, the cells remained stable for over 500 cycles with Coulombic efficiencies of as high as 99.3% and 99.2%, respectively. These high values are higher than that with pure $ZnSO_4$ electrolyte, indicating the enhanced reversibility. Moreover, they are also superior to those with previous reported additives under the similar conditions, such as anti-solvent (99.1%), Na_4EDTA additive (98.4%), GO additive (99.1%), glucose additive (97.3%).[5a,6b,7a,c,f] The successfully boosted performance confirms that these two additives significantly improve battery stability, aligning well with the predictions of their optimal partitions and demonstrating the effectiveness and practicality of our AI model. A recent study by Cao et al.[19] also investigates the enhancement role of acetone in AZIBs, further supporting our predictions. Moreover, the cycled Zn morphology was analyzed using a scanning electron microscope (SEM), as shown in Figure 4e–g. In the pure $ZnSO_4$ electrolyte (Figure 4e), the cycled Zn electrode displays prominent hexagonal plates and clusters, which correspond to the formation of $Zn_4SO_4(OH)_6{\cdot}xH_2O$ by-products and Zn dendrites during cycling. These corrosion by-products and dendrites significantly diminish the Zn reversibility and overall cycling stability, highlighting the challenges posed by the pure electrolyte. In sharp contrast, the Zn electrodes cycled in electrolytes with the acetone and butanetriol additives (Figure 4f,g) exhibit smooth and clean surfaces, with no visible dendrite formation. This morphological improvement clearly demonstrates the effectiveness of these additives in suppressing the side reactions and preventing the growth of Zn dendrites, ultimately leading to enhanced cycling stability and better battery performance. The clean surface and absence of detrimental growth further underscore the protective role of the additives in stabilizing the Zn anodes during battery cycling.

3. Conclusion

In summary, we report an AI-assisted methodology for screening additive molecules to design advanced electrolyte systems that enhance the stability of AZIBs. By benchmarking with experimentally measured Coulombic efficiency results, we

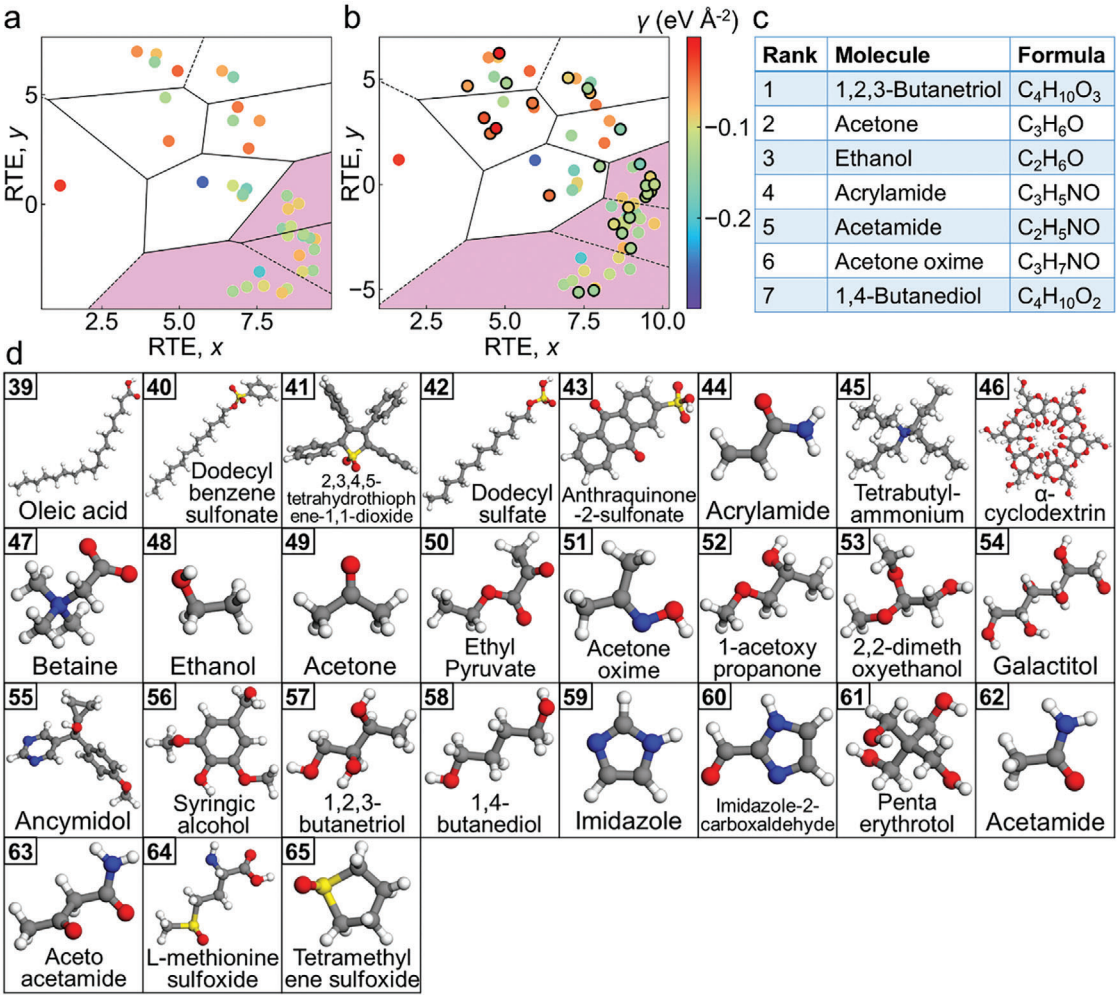

Rank	Molecule	Formula
1	1,2,3-Butanetriol	$C_4H_{10}O_3$
2	Acetone	C_3H_6O
3	Ethanol	C_2H_6O
4	Acrylamide	C_3H_5NO
5	Acetamide	C_2H_5NO
6	Acetone oxime	C_3H_7NO
7	1,4-Butanediol	$C_4H_{10}O_2$

Figure 3. Map for electrolyte additive selection based on physical properties. a,b) Dimensionality reduction using the random trees embedding (RTE) algorithm and Voronoi partitioning using K-Means clustering for the a) training dataset and b) combined training and prediction dataset. The ML predicted data points are distinguished by black circles. Colors represent surface free energies (γ). The obtained optimal region for enhancing battery stability is shown in light purple. c) Top 50% additive molecules in the optimal region, ranked by γ from negative to positive. d) 27 additive molecules as the ML prediction set. C, grey small spheres; O, red small spheres; N, blue small spheres; S, yellow small spheres; H, white small spheres.

established an additive molecule model with full coverage of an explicit water solvent on the Zn(002) surface and used DFT to calculate its surface free energy as a reliable descriptor of Zn reversibility. A database was created using 38 additive molecules compressed from extensive literature, incorporating up to 17 experimentally measurable physical quantities from these molecules as features for ML training. The RTE dimensionality reduction algorithm generated a 2D mapping to visualize the effects of these physical quantities, which was combined with an AI clustering method to classify the molecules and identify partitions with better performance in AZIBs. From the best partitions, 1,2,3-butanetriol and acetone were selected as the effective additive molecules for enhancing AZIB stability, and their effectiveness was successfully verified experimentally. Growing number of studies in recent years validate AI predictions through experiments, offering support for this research paradigm.[20] Future work will focus on merging molecular design from a structural perspective[21] with practical application descriptors, combining the generated models to further improve electrolyte molecule design. This strategy, which well integrates DFT computational simulation, large-scale experimental data analysis, and AI-assisted design, can be extended to other molecular design-related systems and guide the development of future battery electrolyte.

4. Experimental Section

DFT Computations: DFT computations were performed using the Vienna ab initio simulation package (VASP),[22] projector-augmented wave (PAW)[23] pseudopotentials, and the Perdew-Burke-Ernzerhof (PBE)[24] exchange-correlation functional, with the DFT-D3[25] method for van der Waals correction. The plane wave cutoff was set to 600 eV. All atoms were fully relaxed until convergence of energy, and forces were 1×10^{-5} eV and 0.05 eV $Å^{-1}$, respectively. Zn bulk structure was computed with a $12 \times 12 \times 12$ *k*-grid. For computations for Zn(002) surface structures, the unit-cell size was (10.46 × 10.46) Å, the vacuum layer was 20 Å and a $2 \times 2 \times 1$ *k*-grid was used. The surface model contains four Zn atomic layers, with the

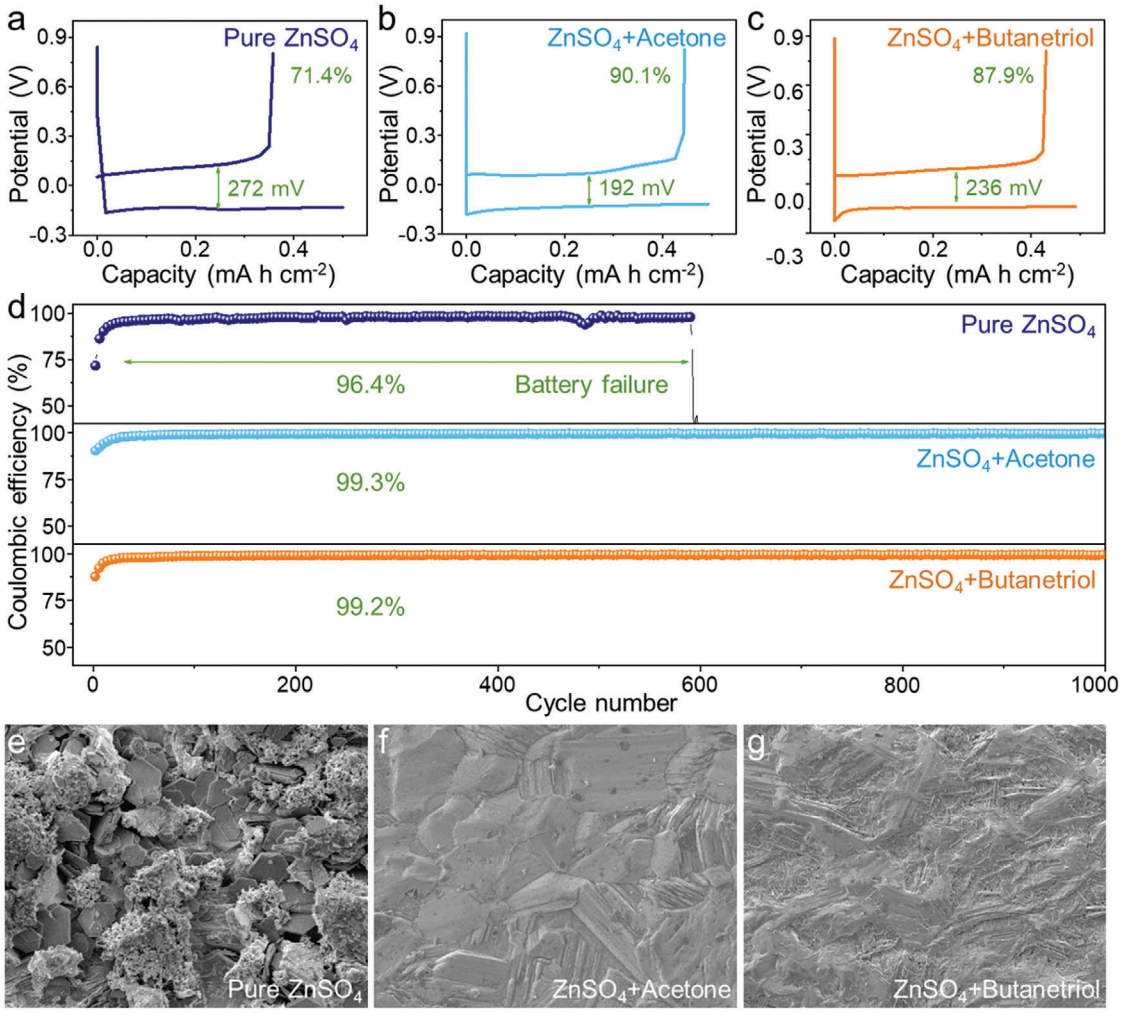

Figure 4. Experimental performance for AZIBs with different additives. a–c) Initial charge-discharge voltage profiles of cells using pure $ZnSO_4$ electrolyte (a), $ZnSO_4$ electrolyte with acetone additive (b), and $ZnSO_4$ electrolyte with 1,2,3-butanetriol additive (c). d) Cycling stability of cells using pure $ZnSO_4$ electrolyte, and $ZnSO_4$ electrolyte with acetone and 1,2,3-butanetriol additives. e–g) Scanning electron microscope (SEM) image of cycled Zn electrode in pure $ZnSO_4$ electrolyte (e), $ZnSO_4$ electrolyte with acetone additive (f), and $ZnSO_4$ electrolyte with 1,2,3-butanetriol additive (g).

bottom two layers kept fixed and the rest atoms fully relaxed. One explicit water layer with 12 H_2O molecules was added on the surface to simulate the aqueous electrolyte environment for surface free energy calculations.

Surface Free Energies and Adsorption Energies: The adsorption energy (E_{ad}) was obtained from:

$$E_{ad} = E_{tot} - E_{surf} - E_{molecule} \quad (1)$$

where E_{tot} was the DFT total energy of the surface with adsorbate, E_{surf} the energy of the bare Zn(002) surface, and $E_{molecule}$ the energy of the additive molecule. More-negative E_{ad} values evidence stronger adsorption.

Within ab initio thermodynamics,[26] the surface free energy (γ) is obtained from:

$$\gamma = \frac{1}{A}\left[G_{surf}(Zn + electrolyte) - G_{surf}(Zn + H_2O) - xE_{molecule}\right] \quad (2)$$

where G_{surf}(Zn+electrolyte) and G_{surf}(Zn+H_2O) was the Gibbs free energy of the Zn(002) surface with aqueous electrolyte containing additive molecules and the Gibbs free energy of Zn(002) surface with water, respectively. These values were approximated by their respective DFT total energies, i.e., $G_{surf} \approx E_{surf}$. $E_{molecule}$ was the energy of the additive molecule. A was the surface unit-cell area. x was the number of additive molecules contained in each unit-cell, which was determined by the size of the molecule. More negative γ values evidence a more-stable surface structure.

ML Prediction: The well-established symbolic regression algorithm SISSO[15] has been used to identify the best sparse solution out of an immense feature space spanned by various nonlinear combinations of primary features. The operators were applied iteratively to the generated feature spaces, with the number of iterations performed, N, being a hyperparameter of the method (denoted the rung, Φ_N). An increase of N leads to a rapidly growing size of the total feature space, which improves the accuracy while increasing the amount of calculation. The SISSO training result was the operation between primary features with fitting coefficients as descriptors to represent the surface free energies (γ). In this work, the Φ_2 feature space with descriptor dimension 4 was used to predict γ, and a 5-fold cross validation was conducted to test the root mean square error (RMSE).

AI Clustering: K-Means[17] was used as the clustering algorithm. The input array was preprocessed using two dimensionality reduction algorithms, random tree embedding (RTE)[16] before being fed into the K-Means algorithm. For both clustering and dimensionality reduction methods, the implementations in the *Scikit-learn*[27] library were used.

K-Means: The number of clusters was set to 9. The initialization of the cluster center plays a crucial role in the final output, and here the "k-means++" initialization method[28] was used. The random-state for centroid initialization was set to 4.

RTE: The number of output dimensions in which to immerse dissimilarities was set to 2. The number of trees in the forest and the maximum depth of each tree was set to 120 and 3, respectively. The random number generator used was controlled to 6.

Experimental Characterization: A 2 M $ZnSO_4$ electrolyte was prepared using $ZnSO_4{\cdot}7H_2O$ and deionized water in a 100-mL volumetric flask. Based on the aqueous $ZnSO_4$ electrolyte, 1,2,3-butanetriol and acetone additives were added to obtained 2 M $ZnSO_4$ + 10 v/v% 1,2,3-butanetriol and 2 M $ZnSO_4$ + 10 v/v% acetone, respectively. Electrochemical characterization of Zn/Cu cells was measured using 2032-type coin-cells with different electrolytes. The Zn plating/stripping was performed at 0.5 mA cm^{-2} with a capacity of 0.5 mA h cm^{-2}. The morphology of Zn electrodes after cycling in different electrolytes was observed by field emission scanning electron microscopy (FESEM, JEOL JSM-7500FA), operated at 5 kV and 10 mA.

Supporting Information

Supporting Information is available from the Wiley Online Library or from the author.

Acknowledgements

H.L. and J.H. contributed equally to this work. Financial support from the Australian Research Council (ARC) (IL230100039, DP220102596, DE240100661, DE230100471) was gratefully acknowledged. DFT computations were undertaken with the assistance of resources and services from the National Computational Infrastructure (NCI) and Phoenix High Performance Computing, which were supported by the Australian Government and the University of Adelaide. The authors acknowledge the Australian Institute of Nuclear Science and Engineering (AINSE) support through Early Career Researcher Grant (ECRG, J.H.). [Correction added on November 30, 2024, after first online publication: Scheme 1 has been replaced.]

Conflict of Interest

The authors declare no conflict of interest.

Data Availability Statement

The data that support the findings of this study are available from the corresponding author upon reasonable request.

Keywords

aqueous battery stability, artificial-intelligence clustering, data-driven machine learning, electrolyte additive design, surface free energy

Received: August 13, 2024
Revised: October 9, 2024
Published online: October 23, 2024

[1] a) J. Hao, S. Zhang, H. Wu, L. Yuan, K. Davey, S.-Z. Qiao, *Chem. Soc. Rev.* **2024**, *53*, 4312; b) D. Chao, W. Zhou, F. Xie, C. Ye, H. Li, M. Jaroniec, S.-Z. Qiao, *Sci. Adv.* **2020**, *6*, eaba4098; c) J. Zhu, Z. Tie, S. Bi, Z. Niu, *Angew. Chem., Int. Ed.* **2024**, *63*, 202403712.

[2] a) Y. Geng, L. Pan, Z. Peng, Z. Sun, H. Lin, C. Mao, L. Wang, L. Dai, H. Liu, K. Pan, X. Wu, Q. Zhang, Z. He, *Energy Storage Mater.* **2022**, *51*, 733; b) T. Zhang, Y. Tang, S. Guo, X. Cao, A. Pan, G. Fang, J. Zhou, S. Liang, *Energy Environ. Sci.* **2020**, *13*, 4625.

[3] a) Z. Zheng, J. Li, Y. Pan, Y. Yu, D. Zhu, J. Prabowo, L. Wei, Y. Chen, *Next Energy.* **2023**, *1*, 100073; b) Y. Du, Y. Li, B. B. Xu, T. X. Liu, X. Liu, F. Ma, X. Gu, C. Lai, *Small.* **2022**, *18*, 2104640; c) Z. Deng, L. Ouyang, L. Ma, L. Yang, M. Zhu, *Curr. Opin. Electrochem.* **2024**, *45*, 101483; d) H. Ren, S. Li, B. Wang, Y. Zhang, T. Wang, Q. Lv, X. Zhang, L. Wang, X. Han, F. Jin, C. Bao, P. Yan, N. Zhang, D. Wang, T. Cheng, H. Liu, S. Dou, *Adv. Mater.* **2023**, *35*, 2208237; e) H. Ren, S. Li, B. Wang, Y. Gong, H. Zhang, J. Wang, Q. Lv, D. Wang, H. Liu, S. Dou, *Energy Storage Mater.* **2024**, *68*, 103364.

[4] a) L. Cheng, R. S. Assary, X. Qu, A. Jain, S. P. Ong, N. N. Rajput, K. Persson, L. A. Curtiss, *J. Phys. Chem. Lett.* **2015**, *6*, 283; b) Y. Xiao, L. J. Miara, Y. Wang, G. Ceder, *Joule.* **2019**, *3*, 1252; c) H. Li, X. Li, P. Wang, Z. Zhang, K. Davey, J. Q. Shi, S.-Z. Qiao, *J. Am. Chem. Soc.* **2024**, *146*, 22850.

[5] a) Y. Zhu, J. Hao, Y. Huang, Y. Jiao, *Small Struct.* **2023**, *4*, 2200270; b) Y. Ding, L. Yin, T. Du, Y. Wang, Z. He, J. A. Yuwono, G. Li, J. Liu, S. Zhang, T. Yang, Z. Guo, *Adv. Funct. Mater.* **2024**, *34*, 2314388.

[6] a) Y. Wang, X. Zeng, H. Huang, D. Xie, J. Sun, J. Zhao, Y. Rui, J. Wang, J. A. Yuwono, J. Mao, *Small Struct.* **2024**, *8*, 2300804; b) S.-J. Zhang, J. Hao, D. Luo, P.-F. Zhang, B. Zhang, K. Davey, Z. Lin, S.-Z. Qiao, *Adv. Energy Mater.* **2021**, *11*, 2102010.

[7] a) S. C. Kim, S. T. Oyakhire, C. Athanitis, J. Wang, Z. Zhang, W. Zhang, D. T. Boyle, M. S. Kim, Z. Yu, X. Gao, T. Sogade, E. Wu, J. Qin, Z. Bao, S. F. Bent, Y. Cui, *Proc. Natl. Acad. Sci. USA.* **2023**, *120*, 2214357120; b) Y.-C. Gao, N. Yao, X. Chen, L. Yu, R. Zhang, Q. Zhang, *J. Am. Chem. Soc.* **2023**, *145*, 23764.

[8] a) H. Yang, Y. Che, A. I. Cooper, L. Chen, X. Li, *J. Am. Chem. Soc.* **2023**, *145*, 27038; b) H. Li, Y. Jiao, K. Davey, S.-Z. Qiao, *Angew. Chem., Int. Ed.* **2023**, *62*, 202216383; c) J. Lan, A. Palizhati, M. Shuaibi, B. M. Wood, B. Wander, A. Das, M. Uyttendaele, C. L. Zitnick, Z. W. Ulissi, *npj Comput. Mater.* **2023**, *9*, 172.

[9] a) A. Mazheika, Y.-G. Wang, R. Valero, F. Viñes, F. Illas, L. M. Ghiringhelli, S. V. Levchenko, M. Scheffler, *Nat. Commun.* **2022**, *13*, 419; b) R. Palkovits, S. Palkovits, *ACS Catal.* **2019**, *9*, 8383.

[10] H. Li, Y. Jiang, X. Li, K. Davey, Y. Zheng, Y. Jiao, S.-Z. Qiao, *J. Am. Chem. Soc.* **2023**, *145*, 14335.

[11] a) H. Cao, X. Huang, Y. Li, Y. Liu, Q. Zheng, Y. Huo, R. Zhao, J. Zhao, D. Lin, *Chem. Eng. J.* **2023**, *455*, 140538; b) J. Hao, L. Yuan, C. Ye, D. Chao, K. Davey, Z. Guo, S.-Z. Qiao, *Angew. Chem., Int. Ed.* **2021**, *60*, 7366; c) L. Cao, D. Li, E. Hu, J. Xu, T. Deng, L. Ma, Y. Wang, X.-Q. Yang, C. Wang, *J. Am. Chem. Soc.* **2020**, *142*, 21404; d) J. Shi, K. Xia, L. Liu, Q. Zhang, L. Li, X. Zhou, J. Liang, Z. Tao, *Electrochim. Acta.* **2020**, *358*, 136937; e) Q. Ma, R. Gao, Y. Liu, H. Dou, Y. Zheng, T. Or, L. Yang, Q. Li, Q. Cu, R. Feng, Z. Zhang, Y. Nie, B. Ren, D. Luo, X. Wang, A. Yu, Z. Chen, *Adv. Mater.* **2022**, *34*, 2207344; f) P. Sun, L. Ma, W. Zhou, M. Qiu, Z. Wang, D. Chao, W. Mai, *Angew. Chem., Int. Ed.* **2021**, *60*, 18247.

[12] J. Musielewicz, X. Wang, T. Tian, Z. Ulissi, *Mach. Learn.: Sci. Technol.* **2022**, *3*, 03LT01.

[13] a) Z. Wu, Y. Li, J. Liu, *Small Methods.* **2024**, *8*, 2300660; b) P. Li, Y. Wang, Q. Xiong, Y. Hou, S. Yang, H. Cui, J. Zhu, X. Li, Y. Wang, R. Zhang, S. Zhang, X. Wang, X. Jin, S. Bai, C. Zhi, *Angew. Chem., Int. Ed.* **2023**, *62*, 202303292.

[14] a) Y. Quan, M. Yang, M. Chen, W. Zhou, X. Han, J. Chen, B. Liu, S. Shi, P. Zhang, *Chem. Eng. J.* **2023**, *458*, 141392; b) Z. Chen, H. Chen, Y. Che, L. Cheng, H. Zhang, J. Chen, F. Xie, N. Wang, Y. Jin, H. Meng, *ACS Sustainable Chem. Eng.* **2021**, *9*, 6855; c) F. Zhao, Z. Jing, X. Guo, J. Li, H. Dong, Y. Tan, L. Liu, Y. Zhou, R. Owen, P. R. Shearing, D. J. L. Brett, G. He, I. P. Parkin, *Energy Storage Mater.* **2022**, *53*, 638; d) D. Geng, Y. Tang, X. Han, Z. Cheng, L. Han, J. Liu, *Int. J. Electrochem. Sci.* **2023**, *18*, 100191; e) M. Wang, J. Cheng, H. Zhao, J. Gao, J. Li, Y.

Wang, J. Qiu, H. Zhang, X. Chen, Y. Wei, *Small.* **2023**, *19*, 2302105; f) J. Chen, W. Zhou, Y. Quan, B. Liu, M. Yang, M. Chen, X. Han, X. Xu, P. Zhang, S. Shi, *Energy Storage Mater.* **2022**, *53*, 629; g) F. Yang, J. A. Yuwono, J. Hao, J. Long, L. Yuan, Y. Wang, S. Liu, Y. Fan, S. Zhao, K. Davey, Z. Guo, *Adv. Mater.* **2022**, *34*, 2206754; h) K. Wang, F. Liu, Q. Li, J. Zhu, T. Qiu, X.-X. Liu, X. Sun, *Chem. Eng. J.* **2023**, *452*, 139577; i) K. Zhao, F. Liu, G. Fan, J. Liu, M. Yu, Z. Yan, N. Zhang, F. Cheng, *ACS Appl. Mater. Interfaces.* **2021**, *13*, 47650; j) W. Zhou, M. Chen, Y. Quan, J. Ding, H. Cheng, X. Han, J. Chen, B. Liu, S. Shi, X. Xu, *Chem. Eng. J.* **2023**, *457*, 141328; k) J. Wan, R. Wang, Z. Liu, L. Zhang, F. Liang, T. Zhou, S. Zhang, L. Zhang, Q. Lu, C. Zhang, Z. Guo, *ACS Nano.* **2023**, *17*, 1610; l) B. Raza, A. Naveed, J. Chen, H. Lu, T. Rasheed, J. Yang, Y. Nuli, J. Wang, *Energy Storage Mater.* **2022**, *46*, 523; m) G. Ma, L. Miao, Y. Dong, W. Yuan, X. Nie, S. Di, Y. Wang, L. Wang, N. Zhang, *Energy Storage Mater.* **2022**, *47*, 203; n) W. Zhang, Y. Dai, R. Chen, Z. Xu, J. Li, W. Zong, H. Li, Z. Li, Z. Zhang, J. Zhu, F. Guo, X. Gao, Z. Du, J. Chen, T. Wang, G. He, I. P. Parkin, *Angew. Chem., Int. Ed.* **2023**, *62*, 202212695; o) D. Han, Z. Wang, H. Lu, H. Li, C. Cui, Z. Zhang, R. Sun, C. Geng, Q. Liang, X. Guo, Y. Mo, X. Zhi, F. Kang, Z. Wang, Q.-H. Yang, *Adv. Energy Mater.* **2022**, *12*, 2102982; p) Y. Shang, P. Kumar, T. Musso, U. Mittal, Q. Du, X. Liang, D. Kundu, *Adv. Funct. Mater.* **2022**, *32*, 2200606; q) D. Xie, Y. Sang, D.-H. Wang, W.-Y. Diao, F.-Y. Tao, C. Liu, J.-W. Wang, H.-Z. Sun, J.-P. Zhang, X.-L. Wu, *Angew. Chem., Int. Ed.* **2023**, *62*, 302216934; r) X. Zhao, N. Dong, M. Yan, H. Pan, *ACS Appl. Mater. Interfaces.* **2023**, *15*, 4053; s) H. K. Bezabh, J.-C. Chiou, T. A. Nigatu, T. M. Hagos, S.-K. Jiang, Y. Nikodimos, B. W. Taklu, M.-C. Tsai, W.-N. Su, B. J. Hwang, *ACS Appl. Mater. Interfaces.* **2023**, *15*, 7949; t) J. Yin, H. Liu, P. Li, X. Feng, M. Wang, C. Huang, M. Li, Y. Su, B. Xiao, Y. Cheng, X. Xu, *Energy Storage Mater.* **2023**, *59*, 102800; u) W. He, Y. Ren, B. S. Lamsal, J. Pokharel, K. Zhang, P. Kharel, J. J. Wu, X. Xiao, Y. Cao, Y. Zhou, *ACS Appl. Mater. Interfaces* **2023**, *15*, 6647; v) T. Xin, R. Zhou, Q. Xu, X. Yuan, Z. Zheng, Y. Li, Q. Zhang, J. Liu, *Chem. Eng. J.* **2023**, *452*, 139572; w) C. Wu, C. Sun, K. Ren, F. Yang, Y. Du, X. Gu, Q. Wang, C. Lai, *Chem. Eng. J.* **2023**, *452*, 139465; x) Z. Liu, Y. Yang, S. Liang, B. Lu, J. Zhou, *Small Struct.* **2021**, *2*, 2100119; y) J. Luo, L. Xu, Y. Zhou, T. Yan, Y. Shao, D. Yang, L. Zhang, Z. Xia, T. Wang, L. Zhang, T. Cheng, Y. Shao, *Angew. Chem., Int. Ed.* **2023**, *62*, 202302302; z) H. Cao, X. Huang, Y. Liu, Q. Hu, Q. Zheng, Y. Huo, F. Xie, J. Zhao, D. Lin, *J. Colloid Interface Sci.* **2022**, *627*, 367; aa) A. Naveed, H. Yang, J. Yang, Y. Nuli, J. Wang, *Angew. Chem., Int. Ed.* **2019**, *58*, 2760; ab) J. Yang, Y. Zhang, Z. Li, X. Xu, X. Su, J. Lai, Y. Liu, K. Ding, L. Chen, Y.-P. Cai, Q. Zheng, *Adv. Funct. Mater.* **2022**, *32*, 2209642; ac) W. Xu, K. Zhao, W. Huo, Y. Wang, G. Yao, X. Gu, H. Cheng, L. Mai, C. Hu, X. Wang, *Nano Energy.* **2019**, *62*, 275; ad) X. Gu, Y. Du, Z. Cao, F. Ma, J. Li, Q. Wang, C. Lai, *Chem. Eng. J.* **2023**, *460*, 141902; ae) N. Wang, X. Chen, H. Wan, B. Zhang, K. Guan, J. Yao, J. Ji, J. Li, Y. Gan, L. Lv, L. Tao, G. Ma, H. Wang, J. Zhang, H. Wang, *Adv. Funct. Mater.* **2023**, *33*, 2300795; af) J. Hao, L. Yuan, Y. Zhu, M. Jaroniec, S.-Z. Qiao, *Adv. Mater.* **2022**, *34*, 2206963.

[15] a) R. Ouyang, S. Curtarolo, E. Ahmetcik, M. Scheffler, L. M. Ghiringhelli, *Phys. Rev. Mater.* **2018**, *2*, 083802; b) R. Ouyang, E. Ahmetcik, C. Carbogno, M. Scheffler, L. M. Ghiringhelli, *J. Phys.: Mater.* **2019**, *2*, 024002; c) D. Zhang, H. Li, H. Lu, Z. Yin, Z. Fusco, A. Riaz, K. Reuter, K. Catchpole, S. Karuturi, *Energy Environ. Sci.* **2023**, *16*, 5065.

[16] a) J. Fakcharoenphol, S. Rao, K. Talwar, *J.Comput. Syst. Sci.* **2004**, *69*, 485; b) K. Dhamdhere, A. Gupta, H. Räcke, *Symp. Disc. Algor.: Proc. Sevent. Ann. ACM-SIAM Symp. Disc. Algor.* **2006**, *22*, 61.

[17] J. Macqueen, *5th Berkeley Symp. Math. Statist. Prob.* **1967**, *1*, 281.

[18] a) C. Yuan, H. Yang, *J. Multidiscip. Sci.* **2019**, *2*, 226; b) D. M. Saputra, D. Saputra, L. D. Oswari, presented at Proceedings of the Sriwijaya International Conference on Information Technology and Its Applications (SICONIAN 2019) May **2020**, pp 341.

[19] X. Cao, W. Xu, D. Zheng, F. Wang, Y. Wang, X. Shi, X. Lu, *Angew. Chem., Int. Ed.* **2024**, *63*, 202317302.

[20] a) J. A. Hueffel, T. Sperger, I. Funes-Ardoiz, J. S. Ward, K. Rissanen, F. Schoenebeck, *Science.* **2021**, *374*, 1134; b) M. Zhong, K. Tran, Y. Min, C. Wang, Z. Wang, C.-T. Dinh, P. D. Luna, Z. Yu, A. S. Rasouli, P. Brodersen, S. Sun, O. Voznyy, C.-S. Tan, M. Askerka, F. Che, M. Liu, A. Seifitokaldani, Y. Pang, S.-C. Lo, A. Ip, Z. Ulissi, E. H. Sarget, *Nature.* **2020**, *581*, 178; c) R. Miyazaki, K. S. Belthle, H. Tüysüz, L. Foppa, M. Scheffler, *J. Am. Chem. Soc.* **2024**, *146*, 5433.

[21] a) B. Sanchez-Lengeling, A. Aspuru-Guzik, *Science.* **2018**, *361*, 360; b) Y. Du, A. R. Jamasb, J. Guo, T. Fu, C. Harris, Y. Wang, C. Duan, P. Liò, P. Schwaller, T. L. Blundell, *Nat. Mach. Intell.* **2024**, *6*, 589; c) Y. Yao, H. Oberhofer, *J. Chem. Phys.* **2024**, *161*, 074102.

[22] G. Kresse, J. Furthmüller, *Phys. Rev. B.* **1996**, *54*, 11169.

[23] P. E. Blöchl, *Phys. Rev. B.* **1994**, *50*, 17953.

[24] a) J. P. Perdew, K. Burke, M. Ernzerhof, *Phys. Rev. Lett.* **1997**, *78*, 1396; b) Y. Zhang, W. Yang, *Phys. Rev. Lett.* **1998**, *80*, 890.

[25] S. Grimme, J. Antony, S. Ehrlich, H. Krieg, *J. Chem. Phys.* **2010**, *132*, 154104.

[26] a) K. Reuter, *Catal. Lett.* **2016**, *146*, 541; b) K. Reuter, M. Scheffler, *Phys. Rev. B.* **2001**, *65*, 035406; c) H. Li, K. Reuter, *ACS Catal.* **2022**, *12*, 10506.

[27] F. Pedregosa, G. Varoquaux, A. Gramfort, V. Michel, B. Thirion, O. Grisel, M. Blondel, P. Prettenhofer, R. Weiss, V. Dubourg, J. Vanderplas, A. Passos, D. Cournapeau, M. Brucher, M. Perrot, E. Duchesnay, *J. Mach. Learn. Res.* **2011**, *12*, 2825.

[28] D. Arthur, S. Vassilvitskii, SODA '07: Proceedings of the eighteenth annual ACMSIAM symposium on Discrete algorithms, , New Orleans, LA Jan **2007**, pp 1027.